Accepted Manuscript

https://doi.org/10.1016/j.ssnmr.2018.08.002

D. Jardón-Álvarez and J. Schmedt auf der Günne. Reduction of the temperature gradient in laser assisted high temperature MAS NMR. *Solid State Nucl. Magn. Reson.*, 94:26--30, 2018.

Reduction of the temperature gradients in laser assisted high temperature MAS NMR

Daniel Jardón-Álvarez[a], and Jörn Schmedt auf der Günne[b,*]

Abstract

Laser assisted magic angle spinning (MAS) solid state NMR experiments enable studying physicochemical properties at very high temperatures with high resolution. Large temperature gradients however, can degrade resolution and precision of this technique. Due to the strong temperature dependence of the ^{207}Pb chemical-shift in lead nitrate, a temperature difference along the sample leads to a broadening of the signal. A second moment analysis of the NMR spectra serves as an analytical method to quantify the temperature gradient. We show how an arbitrary line-shape can be decomposed into a set of Gaussian functions from which the 2nd moment is calculated in an analytical fashion which improves the numerical stability of the analysis. It was found that measuring the FID in a non-steady temperature state can reduce the temperature gradient inside the rotor, caused by the single-sided heating.

Keywords: solid-state NMR, very high temperature NMR, laser heating, moment analysis

1. Introduction

High temperature nuclear magnetic resonance (HT NMR) is a useful analytical method for investigating properties of materials from microscopic parameters *in situ*, while they are manifesting properties of interest, such as phase transitions and high temperature phases [1–5]. Further, dynamics can be analyzed in terms of activation energies by analysis of longitudinal relaxation of nuclear magnetization and of exchange rates [1,5–10].

The use of a laser beam as heating source in high temperature magic angle spinning (MAS) NMR was first proposed by Taulelle *et al.* [11] in 1989 and has been gaining increased attention ever since [2,4,6,12–14]. With this method temperatures up to 1200 K in MAS NMR measurements have been reported [12]. Heating through laser irradiation ensures that essentially only the sample and the rotor are heated up, in contrast to heating through the bearing gas [12]. This brings two main advantages, first, a probe with temperature resistant materials is not required, only the MAS

a Universität München (LMU), Department of Chemie Butenandtstraße 5-13, 81377 Munich, Germany
b Universität Siegen, Department Chemie und Biologie, Adolf-Reichwein-Str. 2, 57076 Siegen, Germany
* schmedt_auf_der_guenne@chemie.uni-siegen.de

rotor needs to be modified, second, heating of the solenoid (detection) coil can be avoided, which would otherwise cause a decrease in the signal to noise ratio and require retuning of the probe at different temperatures. On the other hand, laser irradiation has the disadvantage of introducing a large temperature gradient along the sample [13], because the sample container is heated only from a single side. The temperature gradient over the sample further reduces the achievable temperature and eventually also broadens the NMR spectra.

Measuring the temperature of the sample inside the spinning rotor constitutes one of the major difficulties in HT MAS NMR. Conventionally, temperatures are calibrated with NMR measurements of samples which present strong temperature dependent features [15], such as sharp temperature transitions [16], relaxation [12,17], quartz oscillators [18] or, more commonly, a well defined dependence of the chemical-shift with the temperature. Such samples are termed chemical-shift thermometers. Various substances suitable for this purpose have been proposed differing in the temperature range over which they can be applied, the precision of temperature determination and the availability of the materials. For instance, known chemical-shift thermometers are ^{119}Sn of the paramagnetic stannates $Sm_2Sn_2O_7$, $Nd_2Sn_2O_7$, $Y_{1.8}Sm_{0.2}Sn_2O_7$ and $Pr_2Sn_2O_7$ [19,20], ^{79}Br of KBr [17] and ^{207}Pb of $Pb(NO_3)_2$ [21,22] and of $CH_3NH_3PbCl_3$ [15].

In this paper we study the temperature gradient build-up in laser assisted HT MAS NMR by looking at the second moment of ^{207}Pb NMR spectra of $Pb(NO_3)_2$ in a temperature range from 20 to 220 °C. We exploit our understanding of the heat transport mechanism inside the NMR rotor to design a pulse sequence and test the idea of reducing the temperature gradient during the measurement by acquiring the FID in a non-steady temperature state.

2. Methods

2.1. NMR measurements

All NMR experiments were conducted at a magnetic field of 11.7 T on a Bruker Avance III spectrometer with a Bruker Biospin laser MAS probe for 7 mm rotors. A *LIMO 200-F400-DL980*, class 4 laser (980 nm), operated with a diode controller *CS400* from *AMTRON,* was used. The laser is directed to the MAS probe through a fiber, a Bragg-mirror reflects the laser beam onto the bottom of the rotor, which consequently is heated up. A thermocouple measures the temperature of the Bragg-mirror which was kept below 333 K with an independent nitrogen source, to ensure reflection efficiency of the mirror. All measurements were performed at a spinning speed of $\nu_r = 3$ kHz. The bearing and drive pressures are important, since they have an influence on the sample temperature, therefore they were kept constant at 1500 mBar and 500 to 540 mBar, respectively. ^{207}Pb chemical shift values are reported by using the δ scale and are referenced to

$(CH_3)_4Pb$, used as an external reference [23], last delays of 17 s were used for single excitation measurements. 98.6% pure $Pb(NO_3)_2$ from VWR-prolabo was used. Takahasi *et al.* [22] found that the temperature dependence of the isotropic chemical shift of lead nitrate follows the quadratic relation:

$$T = -5.2\times10^{-4}\frac{\mathrm{K}}{\mathrm{ppm}^2}\cdot\delta_{iso}^2 + 1.3\frac{\mathrm{K}}{\mathrm{ppm}}\cdot\delta_{iso} + 303.3\,\mathrm{K} \quad , \qquad (1)$$

note that the shifts are given relative to the isotropic chemical shift at 303.3 K.

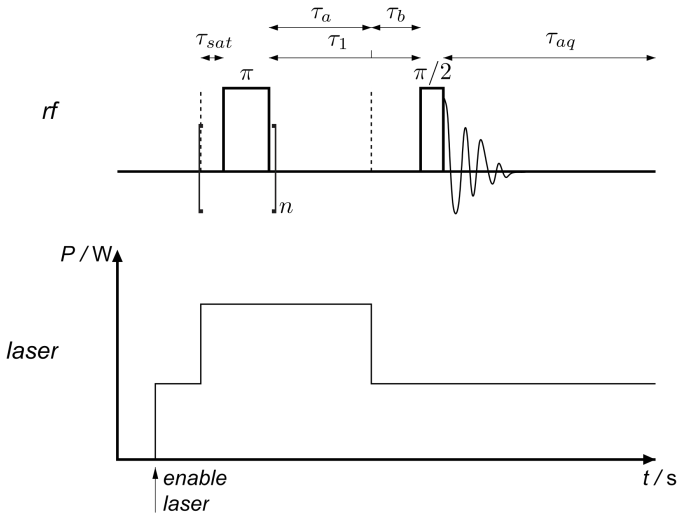

Figure 1: Pulse sequence designed to find the time τ_b in which the temperature gradient in the sample reaches its minimum. The laser is switched between two different powers P_{pulse} and P_{bias}. The variable time τ_b defines the delay between switching down the irradiation power and the $\pi/2$ NMR pulse. A saturation sequence is used to obtain reproducible results. τ_1 is constant and defines the time between the saturation sequence and the $\pi/2$ pulse. After a single $\pi/2$ pulse the FID is measured.

Figure 1 shows the pulse sequence designed to reduce the temperature gradient. Further details on the pulse sequence as well as on the interface between spectrometer and laser unit are given in the *Supporting Information*. This pulse sequence permits acquiring the signal in a non-stationary temperature state. The laser irradiation intensity is switched between two values. During a time τ_a the laser intensity is set at its high value for a sufficiently long time to ensure thermal equilibrium. Subsequently, the laser is switched to a lower value and after a variable time τ_b, a $\pi/2$ NMR pulse is applied and the signal acquired. Note that τ_1 is constant ($\tau_1=\tau_a+\tau_b$). The recycle delay used with this pulse sequence was 16 s.

The design of the insert of the rotors used in the 7 mm laser MAS probe is shown in Fig. 2. The AlN inserts and insert caps are hold by two MACOR rings to an external ZrO_2 spinner, a further zirconia cap (rotor cap) is placed on top of the spinner. This design was conceived to insulate the rotor inserts from the stator. Thereby, cooling of the sample through air flow and a

consequent heating of the stator are reduced. The thermal conductivities of the insert materials differ approximately by two orders of magnitude (from 2 to $2 \cdot 10^2$ $Wm^{-1}K^{-1}$ in ZrO_2 and AlN, respectively [24]). The rotor was packed with two different lead nitrate layers separated by a SiO_2 layer, similar to the packing proposed by Bielecki and Burum [21]. For differentiation, the lower layer had a slightly larger amount of lead nitrate.

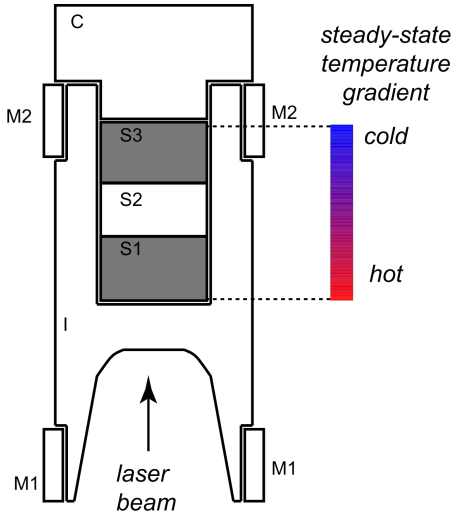

Figure 2: Schematic sketch of a cylindrical insert for 7mm MAS rotors used in the commercial probe head. The laser beam strikes the rotor insert (I) at the bottom. C is the corresponding insert cap, M1 and M2 are the MACOR rings. While heating, a temperature gradient builds up inside the rotor, at a steady state temperature the axial gradient is linear and is represented by the colored bar. The $Pb(NO_3)_2$ sample is arranged into two layers (grey areas, S1 and S3) separated by a SiO_2 layer (white area, S2). This setup was used to experimentally determine the temperature gradient inside the insert.

2.2. Moment analysis

As the resonance frequency of the measured lead nitrate sample is temperature dependent, the broadening of the signal can be used to determine the temperature gradient along the sample. The temperature gradient is likely to cause an asymmetry in the line shape of the NMR signal. In that case, the variance of a single Gaussian/Lorentzian cannot be used as indicator of the line broadening, as it is not possible to accurately fit the spectrum. To overcome this problem, the spectra can be analyzed in terms of the second moment. However, it should be noted that a direct analysis of the second moment from the spectra is not numerically stable. Instead, a stable result can be obtained if the NMR spectrum is deconvoluted into Gaussian functions.

The second moment M_2 about the first moment M_1 is defined as: [25]

$$M_2 = \frac{\int_{-\infty}^{\infty} (x - M_1)^2 f(x)\, dx}{\int_{-\infty}^{\infty} f(x)\, dx} \quad , \qquad (2)$$

with:

$$M_1 = \frac{\int_{-\infty}^{\infty} x f(x)\,dx}{\int_{-\infty}^{\infty} f(x)\,dx} \quad , \tag{3}$$

and the denominator being the total area A_{tot} of $f(x)$. In order to obtain a stable result, the NMR signal has to be deconvoluted, for instance into Gaussian functions. Lorentzian functions are not convenient because their integral over the whole space has no analytical solution. The signal deconvoluted into i Gaussians $G_i(x)$, of area A_i, is defined as:

$$G_i(x) = \sqrt{\frac{b_i}{\pi}}\ \exp\left(-b_i (x - x_{g,i})^2\right) \quad , \tag{4}$$

with b_i being defined through the full width at half height λ_i:

$$b_i = \frac{4\ln(2)}{(\lambda_i)^2} \quad . \tag{5}$$

Making use of the relation that the integral of a sum is equal to the sum over the integrals, the formula for the second moment can be rewritten as

$$M_2 = \sum_i \frac{A_i}{A_{tot}} \int_{-\infty}^{\infty} (x - M_1)^2 G_i(x)\,dx \quad . \tag{6}$$

By analytically solving the integral, the first moment becomes:

$$M_1 = \sum_i \frac{A_i x_{g,i}}{A_{tot}} \quad , \tag{7}$$

and the second moment

$$M_2 = \sum_i \frac{A_i}{A_{tot}} \frac{1 + 2b_i (x_{g,i} - M_1)^2}{2b_i} \quad . \tag{8}$$

This gives an effective and numerically stable analytical way to determine line broadening. Processing of the data was performed with the program *deconv2Dxy* [26]. The square root of the second moment is a direct measure of the signal width, therefore, it was used, instead of the second moment, as a quantitative parameter to compute the temperature gradient inside the rotor.

3. Results and discussion

3.1. Temperature calibration

Lead nitrate ^{207}Pb MAS NMR spectra at different laser beam intensity under continuous laser irradiation are shown in Fig. 3. As previously described, the rotor was packed with two slightly different lead nitrate layers separated by a layer of silica. Due to the temperature gradient inside the rotor the single signal at 0 W splits up into two clearly distinct signals, associated to both layers at higher irradiation powers. The relation between ^{207}Pb isotropic chemical shift of $Pb(NO_3)_2$ and temperature from Takashi *et al.* [22] and given in equation (1) is relative to the chemical shift at 303.3 K. This relation can be generalized to chemical shift values with respect to $(CH_3)_4Pb$ in the

case the temperature for a given chemical shift value is known. For the measurement without laser irradiation we will assume a sample temperature equal to the room temperature of approximately 20 °C, neglecting the heating effects caused by sample spinning. The quadratic equation becomes:

$$T = -5.2\times10^{-4}\,\frac{\mathrm{K}}{\mathrm{ppm}^2}\cdot\delta_{iso}^2 - 2.321\,\frac{\mathrm{K}}{\mathrm{ppm}}\cdot\delta_{iso} - 1474.644\,\mathrm{K} \quad . \qquad (9)$$

Fig. 4 shows the temperatures obtained from the measured chemical shifts for the lead nitrate layer at the bottom of the rotor, plotted against the irradiation power P of the laser beam. It can be seen, that the temperature is nearly linearly dependent on the laser power, within the measured region of up to 500 K, this is in agreement with the observations of Bielecki *et al.* [21]. Only the first two points differ from the trend, which is due to the non-linearity of the laser irradiation at low powers and therefore were not considered for the fit.

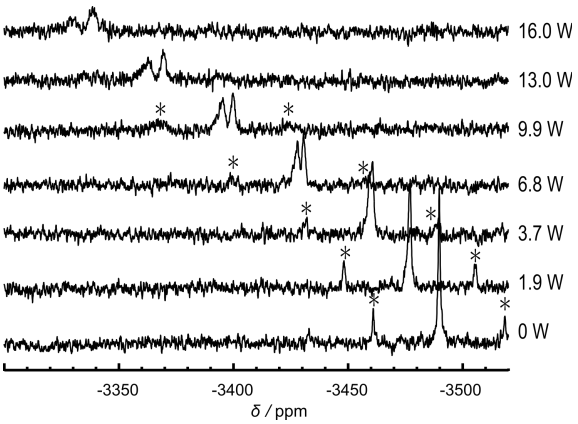

Figure 3: ^{207}Pb single excitation MAS NMR spectra of $Pb(NO_3)_2$ at a rotor spinning speed ν_r of 3 kHz for varying laser beam intensities. The rotor was packed with two slightly different $Pb(NO_3)_2$ layers separated by a SiO_2 layer, as shown in Fig. 2. The rotational side bands are designated by an asterisks.

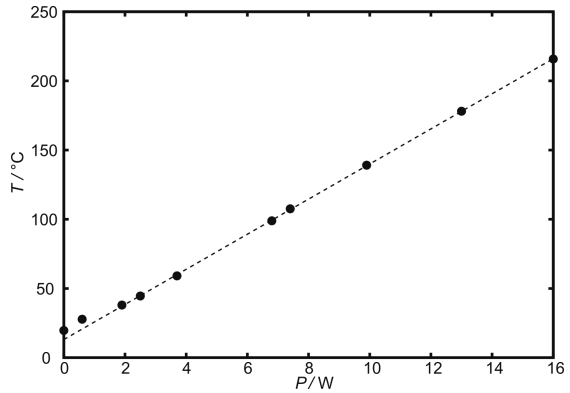

Figure 4: Sample temperature of the ^{207}Pb spectra shown in Fig. 3 for the lead nitrate layer at the bottom of the rotor, calculated according to equation (9), for increasing laser beam powers P. The dashed curve is the function obtained from fitting the data: $T = 12.7\,\frac{\mathrm{K}}{\mathrm{W}}\cdot P + 286.2\,\mathrm{K}$. The asymptotic standard error of the slope of the fitted function is 0.4%.

3.2. Analysis of the temperature gradient

The evolution of the temperature difference between both layers was analyzed from the difference in chemical shift of the NMR signals and is plotted in Fig. 5 for increasing irradiation powers. The temperature gradient increases 0.05 K for every Kelvin heating of the lower layer. The largest observed temperature difference was 10.4 K, which with an approximate distance of 2 mm between the two sheets of $Pb(NO_3)_2$ corresponds to a temperature gradient of 5.2 K/mm. Analysis of the second moment making use of the previously described mathematical framework was done over the entire spectrum. Therefore, the spectra were fitted with one gaussian function for each of the two peaks, from which, upon addition, the total second moment of the spectra could be determined. The calculated square root of the second moments are shown in Fig. 6. Standard deviation of the slope obtained from linear fits was 4 and 7% for ΔT and $(M_2)^{1/2}$, respectively, showing that the second moment is an adequate indicator of the temperature gradient of the sample. Both methods present a linear behavior, implying that the heat transport occurs though a linear mechanism. As no convection is expected for this system and thermal radiation scales with T^4, according to the Stefan-Boltzmann law, we conclude that thermal conduction is the main heat transfer mechanism, following Fourier's law.

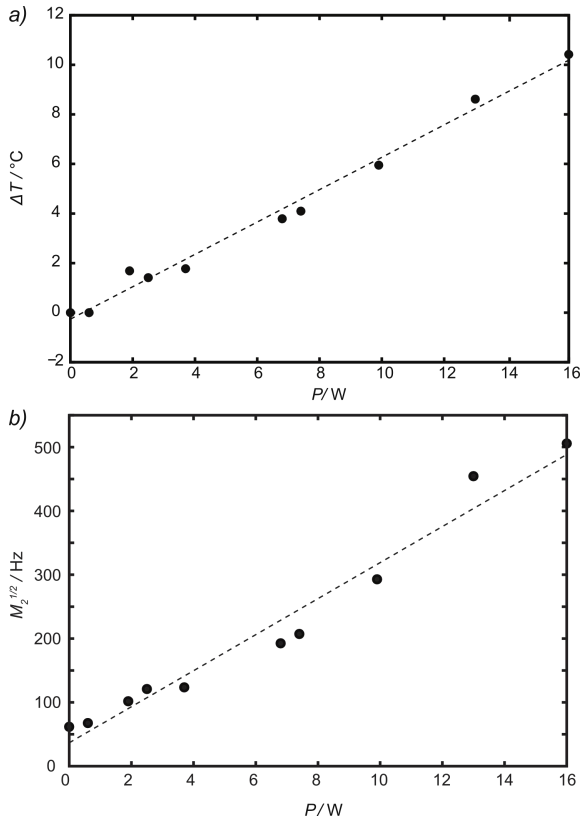

Figure 5: Linear dependencies as a function of the laser irradiation power obtained from the ^{207}Pb spectra shown in Fig. 3 of: a) the temperature differences, ΔT, between the two lead nitrate layers (see Figure 2) and b) the square root of the second moment, $(M_2)^{1/2}$. The dashed curves are the functions obtained from fitting data: a) $\Delta T = 0.64 \frac{\mathrm{K}}{\mathrm{W}} \cdot P$ and b) $(M_2)^{1/2} = 28.24 \frac{\mathrm{Hz}}{\mathrm{W}} \cdot P + 36.61\,\mathrm{Hz}$; the asymptotic standard error of the slopes are 4 and 7%, respectively.

3.3. Gradient reduction

As the temperature gradient is generated from the hot spot, through thermal conduction of sample and rotor insert, it should be possible to reduce the gradient by lifting the condition of measuring under thermal equilibrium. This assumption requires that the upper region of the sample has better isolation compared to the bottom. Therefore, the hot spot will cool fastest, eventually completely inverting the gradient for a period of time. If this is valid, the magnitude of the gradient ideally has to pass through a minimum.

The pulse sequence shown in Fig 1 was first used over a wide range of times τ_b, in order to evaluate the time scale of the temperature setting (not shown) and we observed that the sample temperature had the largest alteration in the order of some few seconds. As the length of the recorded FID is in the order of milliseconds, it can be stated that temperature changes during acquisition are negligible. Subsequently, $Pb(NO_3)_2$ (packed inside the rotor in two layers, as shown in Fig. 2) was measured at various times τ_b, up to 17.5 s, the results are shown in Fig. 6. In the

spectra at τ_b of 2.5, 5 and 7.5 s the otherwise strongly differing signals are considerably overlapped, confirming that both layers cool at different rates. The square root of the second moment obtained from the spectra are plotted as a function of the delay τ_b in Fig. 7. While the second moment of the measurement at $\tau_b = 7.5$ s clearly shows a minimum, already visible by looking at the spectra, a more careful analysis is necessary in order to consider the concurrent reduction of the temperature gradient due to the overall temperature reduction of the system.

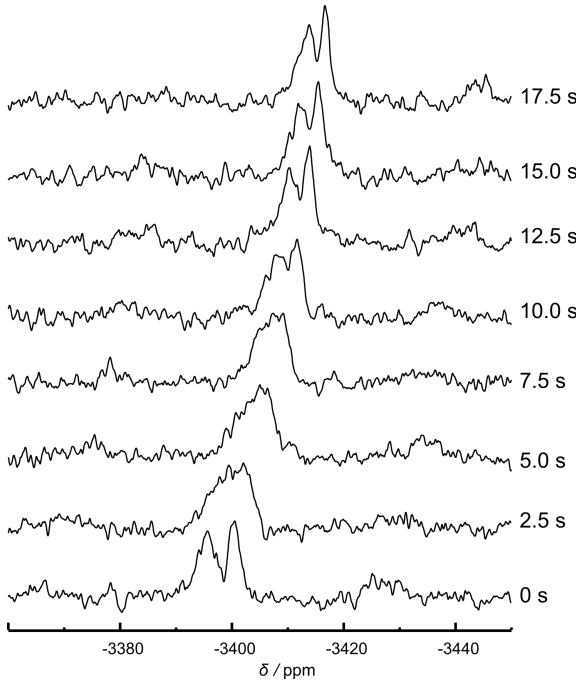

Figure 6: ^{207}Pb spectra of $Pb(NO_3)_2$ (packed as shown in Figure 2) at different cooling times τ_b, according to the pulse sequence shown in Figure 1. The pulse power of the laser was 9.9 W and the bias power 7.4 W. The sample was rotated at a spinning speed ν_r of 3 kHz.

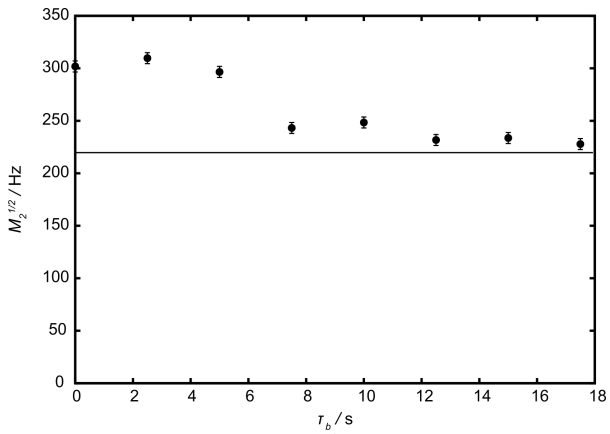

Figure 7: Square root of the second moments $(M_2)^{1/2}$ from the spectra shown in Figure 6. The error bars were set to ±5 Hz from experience. The line at 219.7 Hz is the second moment of a spectrum taken after a τ_b of 5 minutes.

From the obtained first moments we calculated the second moment expected to those values in the stationary case. Square root of expected and experimental second moments are plotted

together in Fig. 8. At 7.5 s we observe a strong reduction of the second moment, meaning that the temperature gradient was successfully reduced with the presented pulse sequence. At this temperature, the gain corresponds to a reduction of the temperature difference among both layers of 15%. For larger delays the gradient slowly approaches the equilibrium value.

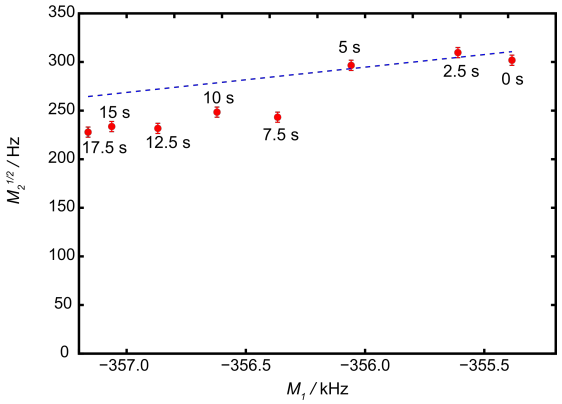

Figure 8: Square root of the second moment $(M_2)^{1/2}$ of the ^{207}Pb lineshape as a function of its first moments M_1. The second moment serves as a measure of the temperature gradient, while the 1st moment is a measure of the average temperature of the sample. Values from the spectra obtained with the pulse sequence shown in Figure 1 for different delays τ_b (time between pulse power reduction and NMR acquisition, and given next to each point), are plotted as red dots. Expected (in a steady state) square roots of the second moment $(M_2)^{1/2}$ at the given first moment, i.e. average sample temperature, calculated from (9) and the linear fits given in the caption of Fig. 5 are shown as blue dashed line. The error bars of the red squares were set from experience.

4. Conclusions

In this paper we present a study of the heating process of laser assisted high temperature MAS NMR. The analysis of spectra in terms of the second moment permits a consistent examination of the temperature gradient, which is the major weakness of laser assisted HT NMR. Understanding the heat transport mechanism inside the NMR rotor allowed us to elaborate a strategy to reduce the large temperature gradient, consisting in making the NMR measurements in a non-steady state. A simple and easy to implement pulse sequence to reduce the temperature difference along the sample is presented and was applied on the chemical shift thermometer lead nitrate, successfully showing a considerable reduction of the temperature gradient.

Acknowledgements

We would like to thank Professor Wolfgang Schnick for giving access to the NMR spectrometer and LASER MAS probehead.

References

[1] J.F. Stebbins, Nuclear Magnetic Resonance at High Temperature, Chem. Rev. 91 (1991) 1353–1373. doi:10.1021/cr00007a004.

[2] S. Wegner, L. van Wüllen, G. Tricot, The structure of phosphate and borosilicate glasses and their structural evolution at high temperatures as studied with solid state NMR spectroscopy: Phase separation, crystallisation and dynamic species exchange, Solid State Sci. 12 (2010) 428–439. doi:10.1016/j.solidstatesciences.2009.03.021.

[3] B. Coté, D. Massiot, F. Taulelle, J.-P. Coutures, ^{27}Al NMR spectroscopy of aluminosilicate melts and glasses, Chem. Geol. 96 (1992) 367–370. doi:10.1016/0009-2541(92)90065-D.

[4] M. Mangstl, J. Weber, D. Jardón Álvarez, O. Burghaus, B. Roling, J. Schmedt auf der Günne, Investigation of bistetramethylammonium hydrogencyclotriphosphate - a molecular rotor?, Chem. - A Eur. J. (2018). doi:10.1002/chem.201800980.

[5] K.K. Inglis, J.P. Corley, P. Florian, J. Cabana, R.D. Bayliss, F. Blanc, Structure and Sodium Ion Dynamics in Sodium Strontium Silicate Investigated by Multinuclear Solid-State NMR, Chem. Mater. 28 (2016) 3850–3861. doi:10.1021/acs.chemmater.6b00941.

[6] M.T. Dunstan, J.M. Griffin, F. Blanc, M. Leskes, C.P. Grey, Ion Dynamics in Li_2CO_3 Studied by Solid-State NMR and First-Principles Calculations, J. Phys. Chem. C. 119 (2015) 24255–24264. doi:10.1021/acs.jpcc.5b06647.

[7] K. Kanehashi, J.F. Stebbins, In situ high temperature ^{27}Al NMR study of structure and dynamics in a calcium aluminosilicate glass and melt, J. Non. Cryst. Solids. 353 (2007) 4001–4010. doi:10.1016/j.jnoncrysol.2007.06.030.

[8] D. Brinkmann, NMR Studies of Superionic Conductors, Prog. Nucl. Magn. Reson. Spectrosc. 24 (1992) 527–552. doi:10.1016/0079-6565(92)80009-5.

[9] J. Emery, O. Bohnke, P. Florian, K. Marzouk, NMR Study of Li^+ Ion Dynamics in the Perovskite $Li_{3x}La_{1/3-x}NbO_3$, J. Phys. Chem. B. 109 (2005) 20680–20689. doi:10.1021/jp051370i.

[10] H. Kirchhain, J. Holzinger, A. Mainka, A. Spörhase, S. Venkatachalam, A. Wixforth, L. van Wüllen, High-temperature MAS-NMR at high spinning speeds, Solid State Nucl. Magn. Reson. 78 (2016) 37–39. doi:10.1016/j.ssnmr.2016.06.003.

[11] F. Taulelle, J.P. Coutures, D. Massiot, J.P. Rifflet, High and very high temperature NMR, Bull. Magn. Reson. 11 (1989) 318–320.

[12] L. van Wüllen, G. Schwering, E. Naumann, M. Jansen, MAS-NMR at very high temperatures, Solid State Nucl. Magn. Reson. 26 (2004) 84–86. doi:10.1016/j.ssnmr.2004.03.001.

[13] H. Ernst, D. Freude, T. Mildner, I. Wolf, Laser-supported high-temperature MAS NMR for time-resolved in situ studies of reaction steps in heterogeneous catalysis, 6 (1996) 147–156.

[14] L. Muñoz-Senovilla, S. Venkatachalam, F. Muñoz, L. Van Wüllen, Relationships between fragility and structure through viscosity and high temperature NMR measurements in Li_2O–ZnO–P_2O_5 phosphate glasses, J. Non. Cryst. Solids. 428 (2015) 54–61.

doi:10.1016/j.jnoncrysol.2015.08.006.

[15] G.M. Bernard, A. Goyal, M. Miskolzie, R. Mckay, Q. Wu, R.E. Wasylishen, V.K. Michaelis, Methylammonium lead chloride : A sensitive sample for an accurate NMR thermometer, J. Magn. Reson. 283 (2017) 14–21. doi:10.1016/j.jmr.2017.08.002.

[16] J. Wu, N. Kim, J.F. Stebbins, Temperature calibration for high-temperature MAS NMR to 913 K: ^{63}Cu MAS NMR of CuBr and CuI, and ^{23}Na MAS NMR of $NaNbO_3$, Solid State Nucl. Magn. Reson. 40 (2011) 45–50. doi:10.1016/j.ssnmr.2011.04.004.

[17] K.R. Thurber, R. Tycko, Measurement of sample temperatures under magic-angle spinning from the chemical shift and spin-lattice relaxation rate of ^{79}Br in KBr powder, J. Magn. Reson. 196 (2009) 84–87. doi:10.1016/j.jmr.2008.09.019.

[18] G. Simon, Quartz Crystal Temperature Sensor for MAS NMR, 198 (1997) 194–198.

[19] C.P. Grey, A.K. Cheetham, C.M. Dobson, Temperature-Dependent Solid-State ^{119}Sn MAS NMR of $Nd_2Sn_2O_7$, $Sm_2Sn_2O_7$, and $Y_{1.8}Sm_{0.2}Sn_2O_7$. Three Sensitive Chemical-Shift Thermometers, J. Magn. Reson. Ser. A. 101 (1993) 299–306. doi:10.1006/jmra.1993.1046.

[20] G.J.M.P. van Moorsel, E.R.H. van Eck, C.P. Grey, $Pr_2Sn_2O_7$ and $Sm_2Sn_2O_7$ as High-Temperature Shift Thermometers in Variable-Temperature ^{119}Sn MAS NMR, J. Magn. Reson. Ser. A. 113 (1995) 159–163. doi:10.1006/jmra.1995.1075.

[21] A. Bielecki, D.P. Burum, Temperature Dependence of ^{207}Pb MAS Spectra of Solid Lead Nitrate. An Accurate, Sensitive Thermometer for Variable-Temperature MAS, J. Magn. Reson. Ser. A. 116 (1995) 215–220. doi:10.1006/jmra.1995.0010.

[22] T. Takahashi, H. Kawashima, H. Sugisawa, B. Toshihide, ^{207}Pb chemical shift thermometer at high temperature for magic angle spinning experiments, Solid State Nucl. Magn. Reson. 15 (1999) 119–123. doi:10.1016/S0926-2040(99)00039-9.

[23] R.K. Harris, E.D. Becker, S.M. Cabral de Menezes, R. Goodfellow, P. Granger, NMR Nomenclature: Nuclear Spin Properties and Conventions for Chemical Shifts, Solid State Nucl. Magn. Reson. 22 (2002) 458–483. doi:10.1006/snmr.2002.0063.

[24] M.W. Barsoun, Fundamentals of Ceramics, 2nd ed., Institute of Physics, Bristol, 2003.

[25] C.P. Slichter, Principles of Magnetic Resonance, 1st ed., Harper & Row, New York, 1963.

[26] J. Schmedt auf der Günne, Deconv2Dxy version 0.5, a line-shape deconvolution program, https://www.chemie-biologie.uni-siegen.de/ac/jsadg/software/deconv2dxy.html.